



Quantum sensor networks as exotic field telescopes for multi-messenger astronomy

Conner Dailey 1, Colin Bradley, Derek F. Jackson Kimball 2, Ibrahim A. Sulai, Szymon Pustelny, Arne Wickenbrock⁵ and Andrei Derevianko ¹⁰

Multi-messenger astronomy, the coordinated observation of different classes of signals that originate from the same astrophysical event, provides a wealth of information about astrophysical processes¹. So far, multi-messenger astronomy has correlated signals from known fundamental forces and standard model particles like electromagnetic radiation, neutrinos and gravitational waves. Many of the open questions of modern physics suggest the existence of exotic fields with light quanta (with masses $\ll 1$ eV c^{-2}). Quantum sensor networks could be used to search for astrophysical signals that are predicted by theories beyond the standard model² that address these questions. Here, we show that networks of precision quantum sensors that, by design, are shielded from or are insensitive to conventional standard model physics signals can be a powerful tool for multi-messenger astronomy. We consider the case in which high-energy astrophysical events produce intense bursts of exotic low-mass fields (ELFs), and we propose a novel model for the potential detection of an ELF signal on the basis of general assumptions. We estimate ELF signal amplitudes, delays, rates and distances of gravitational-wave sources to which global networks of atomic magnetometers3-5 and atomic clocks6-8 could be sensitive. We find that such precision quantum sensor networks can function as ELF telescopes to detect signals from sources that generate ELF bursts of sufficient intensity.

Bursts of exotic low-mass fields (ELFs) could be generated by cataclysmic astrophysical events, such as black-hole or neutron-star mergers9, supernovae10 or the processes that produce fast radio bursts¹¹. Ultralight bosons, which are considered as possible ELFs, have small masses, and therefore a high-energy event is not required for their production. Quantum sensors such as atomic clocks⁶ and magnetometers³ are sensitive to gentle perturbations of internal degrees of freedom (energy levels, spins and so on) by coherent, classical waves. This contrasts with particle detectors, such as those employed in observations of cosmic neutrinos and searches for weakly interacting massive particles. Importantly, the astrophysical source must produce coherent ELF waves with a high-mode occupation number to be detected by these quantum sensors. An axion burst that produces just a few axions that reach Earth would not be detectable with clocks and magnetometers. Therefore, we focus our attention on coherent production mechanisms for ELFs9, rather than thermal (incoherent) production mechanisms¹⁰.

Consider the potential ELF production by binary black hole (BBH) and binary neutron star (BNS) mergers. Much of the underlying physics of coalescing singularities in black-hole mergers remains unexplored, as it requires the understanding of the unknown theory of quantum gravity¹². However, exotic scalar fields also appear in theories that do not require the invocation of quantum gravity, itself. For example, rotating black holes may be surrounded by dense clouds of exotic bosons (with up to 10% of the black-hole mass extracted by the clouds) that could lead to ELF bursts coincident with gravitational-wave emission^{9,13,14}. Scalar fields appear in well-posed theories of scalar-tensor gravity¹⁵, such that black holes and neutron stars are immersed in scalar fields. Modes of these fields can be excited during BBH or BNS mergers¹⁶. Scalar emission can be enhanced substantially by dynamic scalarization¹⁷ and by its monopole character¹⁸.

Given the variety of unconstrained scenarios for ELF emission, we take a pragmatic observational approach on the basis of energy arguments. Gravitational-wave events, which are detectable with present and future gravitational-wave observatories, can radiate great amounts of energy, a fraction of which, ΔE , could be emitted in the form of ELFs. The radiated energy in the form of gravitational waves from recently observed BBH mergers is a few solar masses $(M_{\odot}c^2)$ (refs. ^{19,20}), whereas for recently observed BNS mergers, the radiated energy in the form of gravitational waves is $\gtrsim 0.025 \ M_{\odot}c^2$ (ref. ²¹). For the purposes of the following sensitivity estimates, we assume that it may be possible to have $\Delta E \approx M_{\odot}c^2$ of energy released in the form of ELFs from a black-hole merger and $\Delta E \approx 0.1 \ M_{\odot}c^2$ of energy released in the form of ELFs from a BNS merger. These estimates are on the basis of the idea that the energy released through another channel (ELFs instead of gravitational waves) could be on the order of the measurement uncertainty without altering the 'conventional physics' interpretation of the event.

For concreteness, we assume that the emitted ELF is a spin-0 field, $\phi(r, t)$, which is described by a superposition of spherically symmetric wave solutions to the Klein-Gordon equation, $\phi_k(r,t) = \frac{A_k}{r}\cos(kr - \omega t + \theta_k)$, where r is the radial coordinate, and A_k , θ_k , k and ω are the ELF amplitudes, phases, wavevectors and frequencies, respectively. The spherically symmetric monopole emission pattern is characteristic of scalar-tensor gravity models¹⁸. The ELF frequency ω and wavevector k satisfy the relativistic energy–momentum dispersion relation, $\omega(k) = \sqrt{\left(ck\right)^2 + \Omega_c^2}$, where the Compton frequency $\Omega_c = mc^2/\hbar$ for the ELF mass m. We consider ELFs that are sufficiently far from the source such that general relativistic effects (such as the gravitational redshift) can be ignored. We ignore the effects of Galactic dust on the propagation and attenuation of the ELF waves, also.

Department of Physics, University of Nevada, Reno, NV, USA. Department of Physics, California State University, East Bay, Hayward, CA, USA.

³Department of Physics and Astronomy, Bucknell University, Lewisburg, PA, USA. ⁴Institute of Physics, Jagiellonian University in Kraków, Kraków, Poland.

⁵Helmholtz Institute Mainz, Johannes Gutenberg University, Mainz, Germany. [™]e-mail: andrei@unr.edu

LETTERS NATURE ASTRONOMY

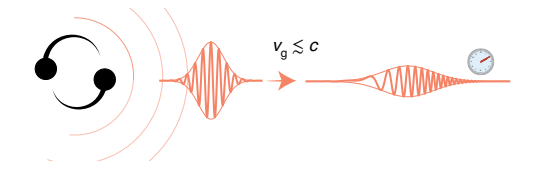


Fig. 1 | Effect of dispersion on the expected ELF signal at a precision quantum sensor. A schematic of the production, propagation and detection of an ELF wave packet (shown in red). A BBH merger (left) emits a burst of ELFs and gravitational waves. As the ELF burst propagates with the group velocity $v_{\rm g} \lesssim c$ to the detector (right), it lags behind the emitted gravitational waves, which propagate at c. Given that the more energetic ELF components propagate faster, the detected ELF wave packet exhibits a characteristic frequency chirp, depicted by the wave packet shown on the right.

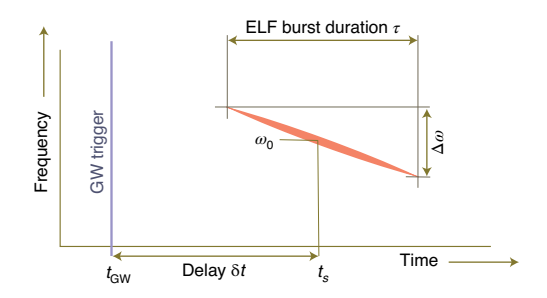


Fig. 2 | Time-frequency decomposition for power spectrum of an ELF signal at a sensor. This template is for interactions with a sensor that are linear in the ELF. The spectral width of the pulse $\Delta\omega$ is related to the initial pulse duration τ_0 as $\Delta\omega=1/\tau_0$. The frequency slope is $\mathrm{d}\omega(t)/\mathrm{d}t=-\Delta\omega/\tau$. For interactions that are quadratic in the ELF, both the central frequency ω_0 and the slope are doubled.

We consider an emitted ELF burst of central frequency ω_0 and of a finite duration τ_0 that has a bandwidth $\Delta\omega\approx 1/\tau_0$, or, equivalently, a characteristic energy $\varepsilon_0=\hbar\omega_0$ and width $\Delta\varepsilon$. Individual Fourier components propagate with different phase velocities as dictated by the dispersion relation, and we expect qualitatively a frequency-chirped ELF signal at the detector, as shown in Figs. 1 and 2. The slope of the chirp is $\mathrm{d}\omega/\mathrm{d}t\approx -\Delta\omega/\tau$, because the frequency content of a wave packet is preserved, owing to energy conservation. Further discussion and calculations are given in the Methods and the Supplementary Information.

With R as the distance from the astrophysical source to the sensor, the time delay between the ELF and gravitational waves (GW) is $\delta t = (R/c)(c/v_g - 1)$, where v_g is the group velocity of the ELF pulse. In this formula, the wave packet propagates over time $t_{GW} = R/c$, which is roughly a billion years for GW150914 (ref. 19). Therefore, $t_{\rm GW}$ is much larger than any reasonably observable time delay in an experiment (for example, $\delta t < 1$ week). Therefore, $(c/v_g - 1) \ll 1$, and ELFs must be ultrarelativistic to be observed. In this limit, photonic dispersion $\omega_0 \approx ck_0$ relates the ELF central frequency ω_0 to the wavevector k_0 . The bandwidth of a quantum sensor fixes measurable ELF frequencies. For atomic clocks, $\omega_0/2\pi \lesssim 1$ Hz, for atomic magnetometers, $\omega_0/2\pi \lesssim 100$ Hz, and for optical cavities, $\omega_0/2\pi \lesssim 10$ kHz. These frequencies fix energies ε_0 of detectable ELFs to less than 10⁻¹⁴ eV for clocks and 10⁻¹⁰ eV for cavities. As the dominant fraction of these energies is kinetic, the fields are necessarily ultralight, $mc^2 \ll \varepsilon_0$. Emitted ELFs are copious ($\gtrsim 10^{70}$ for $\Delta E \approx 0.1 M_{\odot} c^2$ and $\omega_0 = 2\pi \times 10$ kHz). The mode occupation numbers that result at Earth are macroscopic, and therefore ELFs would act as coherent classical fields at the sensors.

The time delay of the ELF signal with respect to the gravitational-wave burst equals $\delta t = \frac{t_{\rm GW}}{2} (\Omega_{\rm c}/\omega_0)^2$. As $\delta t \ll t_{\rm GW}$, the Compton frequency $\Omega_{\rm c} \ll \omega_0$, which is consistent with ultrarelativistic ELFs. We estimate the duration τ of the ELF pulse at the sensor as $\tau \sim R\Delta v_{\rm g}/c^2$, where the spread in group velocities $\Delta v_{\rm g}/c \approx \partial^2 \omega/\partial k^2/\tau_0$. This leads to a relation between the signal duration and time delay $\tau \approx 2\delta t /(\omega_0 \tau_0)$. Given that our approximations hold for sufficiently sharp ELF spectra, $\omega_0 \tau_0 \gg 1$, we require $\tau \ll \delta t$.

The characteristic ELF amplitude A_{k_0} at the sensor can be estimated by the requirement that the energy of the scalar wave that is stored in a shell of thickness $c\tau$ and radius R is equal to ΔE , for $A_{k_0} \approx \frac{1}{\omega_0} \sqrt{\frac{c\Delta E}{2\pi r}}$. In contrast to dispersionless spherical waves, the

field amplitude at the sensor $\phi(R, t)$ scales as $1/R^{3/2}$, which reflects the additional pulse dispersion.

More detailed considerations (see the Methods) yield the approximate time dependence for an ELF signal at the sensor,

$$\phi(t) \approx \frac{1}{R} \left(\frac{c\Delta E}{2\pi^{3/2} \omega_0^2 \tau} \right)^{1/2} \exp\left(-\frac{(t - t_s)^2}{2\tau^2} \right) \times \cos\left(\omega_0 (t - t_s) - \frac{\omega_0}{4\delta t} (t - t_s)^2 \right)$$
(1)

where $t_s = t_{\rm GW} + \delta t$ is the time of arrival of the centre of the pulse (Fig. 2). Note that the ELF frequency is time dependent, $\omega(t) = (1 - (t - t_s)/(2\delta t))\omega_0$, and exhibits a frequency 'chirp' at the sensor. The waveform, equation (1), is shown in Fig. 1, and its power-spectrum time–frequency decomposition is shown in Fig. 2. The slope of the chirp is given by $d\omega/dt = -1/(\tau \tau_0) = -\omega_0/(2\delta t)$, which is consistent with the qualitative arguments presented earlier in the paper. The excess power statistic can be used in data analysis to search for ELFs (see the Methods).

ELFs can generate signals in quantum sensors via 'portals' between the exotic fields and standard model particles and fields. Portals are a phenomenological gauge-invariant collection of standard model operators that are coupled with operators from the ELF sector². We consider interaction Lagrangians that are linear, $\mathcal{L}^{(1)}$, and quadratic, $\mathcal{L}^{(2)}$, in the ELF ϕ . For magnetometers, $\mathcal{L}^{(1)}_{mag} = f_l^{-1} J^\mu \partial_\mu \phi$ and $\mathcal{L}^{(2)}_{mag} = f_q^{-2} J^\mu \partial_\mu \phi^2$, and for clocks, cavities, interferometers and gravimeters, $\mathcal{L}^{(1)}_{clock} = \sqrt{4\pi}/E_{Pl} \left(-d_{m_e} m_e c^2 \bar{\psi}_e \psi_e + d_e F_{\mu\nu}^2/4\right) \phi$ and $\mathcal{L}^{(2)}_{clock} = \left(-m_e c^2 \bar{\psi}_e \psi_e / \Lambda_{m_e}^2 + F_{\mu\nu}^2/(4\Lambda_\alpha^2)\right) \phi^2$. In these expressions, J^μ is the axial-vector current for standard model fermions, ψ_e is the electron bi-spinor, $F_{\mu\nu}$ is the Faraday tensor, E_{Pl} is the Planck energy, and $f_{l,q}$, d_e , d_{m_e} , Λ_{m_e} and Λ_α are coupling constants. Quadratic interactions appear naturally for ELFs that possess either Z_2 or U(1) intrinsic symmetries²².

The \mathcal{L}_{mag} portals lead to fictitious effective magnetic fields that interact with atomic spins and therefore are detectable with atomic magnetometers⁴. The \mathcal{L}_{clk} portals effectively alter fundamental constants⁷, such as the electron mass m_e and the fine-structure constant α . Such portals can imprint measurable signals in atomic clocks⁷, cavities²³ and atom interferometers^{24,25}. The \mathcal{L}_{clock} portals also modify the Earth's gravitational potential and therefore can be detectable with gravimeters²⁵.

ELFs that interact through any of the enumerated portals would drive frequency-chirped signals in quantum sensors (Figs. 1,2), provided that the sensors have sufficient sensitivity and bandwidth. The coupling strengths determine the relative signal amplitude that is detected by the particular sensor, for a given ELF intensity. We show in the Supplementary Information that the sensors can detect ELF bursts as long as the coupling constants satisfy

$$f_l \lesssim 0.4 \hbar^{3/2} c \frac{\sqrt{N_s}}{\sigma_m(\Delta_t) \sqrt{\Delta_t}} \frac{\sqrt{\Delta E}}{R}$$
 (2)

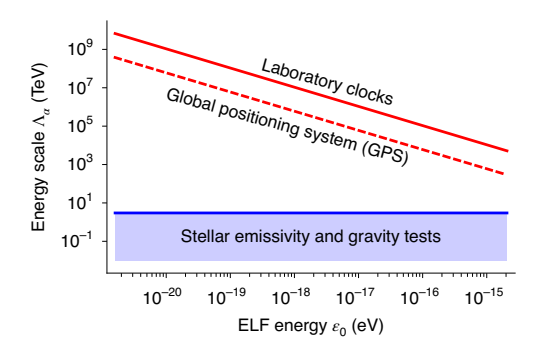


Fig. 3 | Projected atomic-clock sensitivity to ELFs that are plausibly emitted during the BNS merger GW170817. The discovery reach is shown for a trans-European network of laboratory clocks (red line, σ_y (1 s) = 10^{-16}) and for the GPS constellation (red dashed line, σ_y (1 s) = 10^{-13}). We assume an ELF burst of duration $\tau = 100$ s and energy release $0.1 M_{\odot} c^2$, and a total observation time of one month. Prior constraints²⁶ on the energy scale Λ_a are shown by the blue shaded region.

$$f_q \lesssim 0.3 \frac{\hbar c}{R} \left(\frac{N_s}{\Delta_t \tau} \right)^{1/4} \left(\frac{\Delta E}{\sigma_m(\Delta_t) \omega_0} \right)^{1/2} \tag{3}$$

$$d_{X} \gtrsim \frac{E_{\text{Pl}}}{|K_{X}|} \frac{\sigma_{y}(\Delta_{t})}{\sqrt{N_{s}}} \left(\frac{\omega_{0}}{c} R\right) \left(\frac{\Delta_{t}}{\hbar \Delta E}\right)^{1/2} \tag{4}$$

$$\Lambda_X \lesssim 0.2 \left(\frac{\sqrt{N_s} |K_X|}{\sigma_v(\Delta_t)} \right)^{1/2} \left(\frac{c}{R\omega_0} \right) \left(\frac{\hbar^2 \Delta E^2}{\Delta_t \tau} \right)^{1/4}$$
 (5)

Here, K_X is the sensitivity coefficient to a variation in the fundamental constant $X = \{m_e, \alpha, \ldots\}$, Δ_t is the sensor sampling time interval, $\sigma_m(\Delta_t)$ is the magnetometer Allan deviation over Δ_t (in units of energy), $\sigma_y(\Delta_t)$ is the dimensionless clock or interferometer Allan deviation for fractional frequency excursions, and N_s is the number of sensors.

Astrophysical observations and laboratory experiments set constraints on the coupling strengths between ELFs and standard model particles and fields². Using the above sensitivity estimates, we find that for ELFs that couple to standard model particles through the quadratic portal $\mathcal{L}^{(2)}$, the current generation of atomic clocks has an astrophysical reach that spans the observable universe; for the linear portal $\mathcal{L}^{(1)}$, the astrophysical reach of atomic clocks spans only the Milky Way, owing to the fact that prior constraints on linear interactions are much stronger than those for the quadratic portal²⁶.

Several networks of precision quantum sensors are already operational. An example of an atomic-clock network is the Global Positioning System (GPS), which is nominally composed of 32 satellites in medium Earth orbit. The satellites house microwave atomic clocks, and they have been used for dark-matter searches. Combined with other satellite positioning constellations and terrestrial clocks, $N_{\rm s}\approx 100$. Another network is a trans-European fibre-linked network ($N_{\rm s}\approx 10$) of laboratory clocks. As for magnetometers, the Global Network of Optical Magnetometers for Exotic physics (GNOME) targets transient events that are associated with physics beyond the standard model. GNOME is a network of shielded atomic magnetometers that is composed of 13 stations located on four continents. Each station has a magnetometer with subpicotesla sensitivity.

As an example, we plot the projected sensitivity to a putative ELF burst that is emitted during the BNS merger GW170817

(R = 40 Mpc) in Fig. 3. It is clear that existing clock networks can be sensitive to ELFs for a typical gravitational-wave event (BNS, BBH or black-hole-neutron-star mergers) that is registered by gravitational-wave detectors. The case for detection by GPS is particularly intriguing, as roughly 20 years' worth of archival GPS data is available, and the data set is routinely updated. If an ELF signal is discovered in recent data, a search for similar signals prior to the era of the Laser Interferometer Gravitational-wave Observatory (LIGO) can be made in the archival data. Another possibility is to correlate the catalogued short gamma-ray bursts28 or other powerful astrophysical events with the archival GPS data to search for ELF bursts, or even to search for ELF bursts that are uncorrelated with any known astrophysical source. Although estimates show that the existing magnetometer network does not have sufficient sensitivity to probe an unconstrained parameter space for an ELF burst from GW170817 with the assumed characteristics, planned upgrades to GNOME will substantially increase the discovery reach of the network, as discussed in the Supplementary Information.

The employment of networks is crucial to distinguish ELF signals from spurious noise. Furthermore, with baselines of the diameter of Earth or larger, it is possible to resolve the sky position of the ELF source.

The leading edge of an ultrarelativistic ELF burst would propagate across Earth in ~40 ms. At present, GNOME magnetometers have a temporal resolution of ~10 ms; this can be improved to $\lesssim 1$ ms with relatively straightforward upgrades. The angular resolution $\Delta\theta$ based on the ELF time-domain signal pattern is given roughly by the ratio of the temporal resolution to the propagation time through the network: for a temporal resolution of ~1 ms, this corresponds to $\Delta\theta\approx\pi/40$ rad $\approx 2^\circ$. Additionally, given that the ELF gradient points along the ELF velocity vector, the relative signal amplitudes in magnetometers with different sensitive axes enables a second method of angular resolution of the source's sky position. The signal amplitude pattern in the network would yield an angular resolution (in radians) roughly equal to the inverse of the signal-to-noise ratio for the ELF detection.

Unlike magnetometers, atomic clocks and atom interferometers have a relatively low, ~1 Hz, sampling rate. As a result, terrestrial or satellite clock networks cannot be used to track the ELF burst propagation. The ELF propagation time across the GPS constellation is 0.2 s, which is comparable to the 1 s sampling interval in GPS data streams. Nonetheless, clock networks can still act collectively to gain $\sqrt{N_s}$ in sensitivity and disregard signals that do not affect all of the sensors in the network. To mitigate the low sampling rate, the baseline can be increased, similar to recently proposed²⁹ space-based gravitational-wave detectors that rely on atomic clocks and atom interferometers. Another possibility is a small-scale (~10 km) terrestrial network of optical cavities that allow for a ≥10 kHz sampling rate. Each node of such a network would contain two cavities²³, one with a rigid spacer and the other with suspended mirrors. An ELF-induced variation in fundamental constants would change the length and, therefore, the resonance frequency, of the former but not that of the latter. The ELF sensitivity of a cavity network is similar to that of the clock networks shown in Fig. 3.

Methods

Energy density for a spherical wave of an ultrarelativistic scalar field. In the main text, we expand the real-valued scalar field in spherical waves,

$$\phi_k(r,t) = \frac{A_k}{r} \cos(kr - \omega t + \theta_k) \tag{6}$$

Here, r is the radial coordinate, A_k and θ_k are the ELF amplitudes and phases, and k and ω are the ELF wavenumber and oscillation frequency. The field ϕ_k has units of $M^{1/2}L^{1/2}T^{-1}$, and the amplitude A_k has the units of $M^{1/2}L^{1/2}T^{-1}$.

The energy density ρ is given by the 00 component of the stress–energy tensor³⁰,

$$\rho = \frac{1}{2c^2}\dot{\phi}^2 + \frac{1}{2}(\nabla\phi)^2 + \frac{1}{2}\frac{m^2c^2}{\hbar^2}\phi^2 \tag{7}$$

where m is the mass of the scalar. Explicitly, for a spherical wave (equation (6)),

$$\rho = \frac{A_k^2}{2r^2} \frac{\omega^2}{c^2} [\sin^2(\cdots) + \left(\frac{ck}{\omega}\right)^2 \sin^2(\cdots) + \left(\frac{mc^2}{\hbar\omega}\right)^2 \cos^2(\cdots)] + O\left(\frac{1}{r^3}\right) \eqno(8)$$

where '…' stands for the argument of cosine in equation (6). We neglect terms of order $1/r^3$, take the time average over many field oscillations and employ the ultrarelativistic limit, $\omega \approx ck \gg mc^2/\hbar$. The resulting energy density reads

$$\langle \rho \rangle \approx \frac{1}{2} \left(\frac{A_k \, \omega}{r \, c} \right)^2 \tag{9}$$

Dispersion of ultrarelativistic matter wave pulse. Any type of wave will disperse upon propagation, as long as the dispersion relation $\omega(k)$ has a nonzero second derivative with respect to k. This ensures that the group velocity is a function of k. Here, we focus on an analytically tractable case of a Gaussian wave packet that is composed of ultrarelativistic scalar fields.

Dispersion relation in the ultrarelativistic limit. We start with the Klein–Gordon equation for the scalar field $\phi(\mathbf{r},t)$, $(\partial_\mu\partial^\mu+m^2c^2l\hbar^2)\phi(\mathbf{r},t)=0$. We focus on the spherically symmetric solutions (s waves, which are characteristic of scalar emission in scalar–tensor theories) and define $\phi(r,t)=u(r,t)/r$. Then, the Klein–Gordon equation reduces to the one-dimensional wave equation for massive scalar fields

$$\left(\frac{1}{c^2}\frac{\partial^2}{\partial t^2} - \frac{\partial^2}{\partial r^2} + \frac{m^2c^2}{\hbar^2}\right)u(r,t) = 0 \tag{10}$$

Substitution of $u(r,t) \propto \exp(ikr \pm i\omega t)$ leads, as expected, to the relativistic energy-momentum relation

$$\omega(k) = \sqrt{(ck)^2 + (mc^2/\hbar)^2}$$
 (11)

that is, the dispersion relation in the main text. Of course, it holds for waves of arbitrary angular momentum. This dispersion relation may be thought of as giving rise to the 'internal' index of refraction for ELF propagation. In the ultrarelativistic limit, $ck \gg mc^2/\hbar$, the energy of an individual scalar is $\varepsilon \approx c\hbar |k|$.

We can expand $\omega(k)$ further around a characteristic energy $\varepsilon_0 = \hbar \omega_0 \approx c \hbar k_0$,

$$\omega(k) \approx \omega_0 + c \frac{ck_0}{\omega_0}(k - k_0) + \frac{1}{2} \left(\frac{mc^2}{\hbar\omega_0}\right)^2 \frac{c^2}{\omega_0}(k - k_0)^2$$
 (12)

where we keep terms up to second order, only. This parabolic approximation holds as long as $|k-k_0| \ll k_0$, or, equivalently, the energy spectrum of emitted scalars is sufficiently sharp, $\Delta \varepsilon \ll \varepsilon_0$, or $\omega_0 \tau_0 \gg 1$. One can immediately identify the group velocity

$$\frac{v_{\rm g}}{c} = \frac{ck_0}{\omega_0} \approx 1 - \frac{1}{2} \left(\frac{mc^2}{\varepsilon_0}\right)^2 \tag{13}$$

and the characteristic spread in group velocities

$$\frac{\Delta v_{\rm g}}{c} = \left(\frac{mc^2}{\varepsilon_0}\right)^2 \frac{\Delta \varepsilon}{\varepsilon_0} \tag{14}$$

where $\Delta \varepsilon = \hbar/\tau_0$. Finally, the time lag between gravitational-wave and ELF bursts at the sensor a distance R away from the progenitor is

$$\delta t = \left(\frac{mc^2}{\varepsilon_0}\right)^2 \frac{R}{2c} \tag{15}$$

Equations (13)-(15) are the relations used in the main text.

To illustrate the effect of the delay on the detectable ELF mass m, Supplementary Fig. 1 shows the accessible parameter space for an ELF burst that is associated with the GW170608 BBH coalescence event³¹, assuming that the delay δt is less than 10 h.

The general solution to the one-dimensional wave equation is a superposition of waves weighted by Fourier amplitudes a(k),

$$u(r,t) = \frac{1}{\sqrt{2\pi}} \operatorname{Re} \left[\int_{-\infty}^{\infty} a(k) e^{i(kr - \omega(k)t)} dk \right]$$
 (16)

with the dispersion relation (equation (11)). The initial conditions define the Fourier amplitudes $^{\rm 32}$

$$a(k) = \frac{1}{\sqrt{2\pi}} \int_{0}^{\infty} e^{-ikr} \left[u(r,0) + \frac{i}{\omega(k)} \frac{\partial u}{\partial t}(r,0) \right] dr$$
 (17)

where u(r, 0) and $\partial u/\partial t(r, 0)$ are the initial values near the source

Propagation and dispersion of a Gaussian wave packet. We consider a Gaussian wave packet 32 with initial wave amplitude A_0 , initial spatial width L_0 and initial wavevector k_0 .

$$u(r,0) = A_0 e^{-r^2/(2L_0^2)} \cos(k_0 r),$$

$$\frac{\partial u}{\partial x}(r,0) = 0.$$
(18)

The outgoing wave packet has the Fourier amplitude

$$a(k) = \frac{A_0 L_0}{2} e^{-(L_0^2/2)(k - k_0)^2}$$
(19)

which indicates the well-known uncertainty relation between the characteristic spatial extent L_0 of the wave packet and its width in momentum space $\Delta k \approx 1/L_0$. Substitution of the above Fourier amplitude into equation (16) fully solves the problem of propagation. We use the parabolic approximation (equation (12)) for the dispersion relation, which holds as long as $\Delta k \ll k_0$; that is, the characteristic wavelength of the field is much smaller than the initial spatial width L_0 . The parabolic dispersion allows the integral in equation (16) to be evaluated in a closed form.

The final solution for $\phi(r, t)$ reads

$$\phi(r,t) \approx \frac{A_0}{r} \sqrt{\frac{\tau_0}{\tau(t)}} \exp\left(-\frac{(t - r/\nu_{\rm g})^2}{2\tau(t)^2}\right) \cos(\theta(r,t))$$
 (20)

with the time-dependent pulse duration $\tau(t)$ defined as

$$\tau(t) = \sqrt{\tau_0^2 + \left(\frac{\Delta v_g t}{v_g}\right)^2}$$
 (21)

and we have substituted $L_0/\nu_{\rm g}=\tau_0$. The phase argument of the oscillatory part is given by

$$\theta(r,t) = (\omega_0 t - k_0 r) - \frac{1}{2\tau(r)^2} \frac{\Delta v_g t}{v_g \tau_0} (t - r/v_g)^2 + \frac{1}{2} \tan^{-1} \left(\frac{\Delta v_g t}{v_g \tau_0}\right)$$
(22)

In these expressions, group velocity $\nu_{\rm g}$ and its spread $\Delta \nu_{\rm g}$ are given by equations (13) and (14). We focus on the sensor $(t=t_{\rm s}\equiv R/\nu_{\rm g})$ and define the combination

$$\xi = \frac{\Delta v_{\rm g}}{v_{\rm g}} \frac{t_{\rm s}}{\tau_{\rm 0}} = 2 \frac{\delta t}{\tau_{\rm 0}} \frac{\Delta \varepsilon}{\varepsilon_{\rm 0}}$$

where δt is the time lag (equation (15)) between the arrivals of the gravitational-wave and ELF bursts. When $\xi \ll 1$, the duration of the signal at the detector is

$$\tau \approx \frac{\Delta v_{\rm g}}{v_{\rm s}} t_{\rm s} = 2 \frac{\Delta \varepsilon}{\varepsilon_{\rm o}} \delta t \tag{23}$$

Another important feature of the analytical waveform (equation (20)) is that it has an amplitude that scales as $\tau(t)^{-1/2}$, as expected from the total energy conservation arguments of the main text. To relate the amplitude A_0 to the total energy that is released in the ELF channel ΔE , we compute the energy density $\rho(r,t)$ (equation (7)) for the Gaussian wave packet (equation (20)). In the ultrarelativistic limit,

$$\rho(r,t) \approx \frac{1}{2c^2}\dot{\phi}^2 + \frac{1}{2}\left(\frac{\partial\phi}{\partial r}\right)^2 \tag{24}$$

In the evaluation of the derivatives of the field, it is sufficient to keep the derivatives of the rapidly oscillating $\cos(\theta(r,t))$ factor. Then, at a fixed time, we evaluate the pulse energy by the integration of the energy density over the space, which leads to a time-independent value, as expected. From here, we express the amplitude A_0 in terms of the total energy,

$$A_0 \approx \frac{1}{\pi^{1/4}} \left(\frac{1}{\omega_0} \sqrt{\frac{c\Delta E}{2\pi \tau_0}} \right) \tag{25}$$

ELF signal at the sensor. We define the instantaneous frequency $\omega(t) = \mathrm{d}\theta(R, t)/\mathrm{d}t$ and expand it around the time that the centre of the pulse arrives at Earth, $t_s = R/v_g$.

$$\omega(t) \approx \omega(t_s) - \frac{d\omega}{dt}|_{t_s}(t - t_s)$$

$$\approx \omega_0 - \frac{1}{tot}(t - t_s)$$
(26)

The sign of the linear term is consistent with the qualitative expectation that higher frequencies arrive first and lower ones arrive last. The slope of the frequency chirp is given by

$$\frac{\mathrm{d}\omega(t)}{\mathrm{d}t} = -\frac{1}{\tau_0\tau} = -\frac{\omega_0}{2\delta t} \tag{27}$$

Then, at the sensor, the Gaussian ELF burst has an approximate temporal waveform.

$$\phi(t) \approx \frac{A_0}{R} \sqrt{\frac{r_0}{\tau}} \exp\left(-\frac{(t-t_s)^2}{2\tau^2}\right) \times \cos\left(\omega_0(t-t_s) - \frac{\omega_0}{A\delta^2}(t-t_s)^2\right)$$
(28)

or, with equation (25) for the amplitude,

$$\phi(t) \approx \frac{1}{R} \left(\frac{c\Delta E}{2\pi^{3/2} \omega_{0\tau}^{2}} \right)^{1/2} \exp\left(-\frac{(t-t_{\star})^{2}}{2\tau^{2}} \right) \times \cos\left(\omega_{0}(t-t_{\star}) - \frac{\omega_{0\tau}}{2\tau^{2}}(t-t_{\star})^{2} \right)$$
(29)

We show a simulation of such a signal in Supplementary Fig. 2.

General envelope. The preceding analytical results explicitly demonstrate the propagation and dispersion of a Gaussian wave packet. These results hold for a much wider class of sufficiently well-behaved envelopes. Formally, this can be shown by the application of the stationary phase method during the evaluation of the integral in equation (16) for the parabolic dispersion relation (equation (12)). The stationary phase method effectively reduces the wave packet to a Gaussian, and all the derived results immediately apply.

Data analysis considerations. The goal of this section is to outline a data analysis strategy and to establish the projected sensitivity of the proposed search for a generic ELF signal. To reiterate, an arriving ELF wave packet can be characterized by a set of three parameters

$$(\delta t, \tau, \omega_0) \tag{30}$$

that is, by the time delay between gravitational-wave and ELF bursts δt , duration τ and central frequency ω_0 . Notice that the frequency chirp of the pulse is fixed by these parameters through equation (27) (Fig. 2). As our approximations hold for sufficiently sharp ELF spectra, $\omega_0 \tau_0 \gg 1$ (see the previous section), from equation (23), we expect $\tau \ll \delta t$.

Given the parameters (δt , τ , ω_0) and the known gravitational-wave travel time from the progenitor $t_{\rm GW}=R/c$, the other parameters can be fully determined. In particular, the ELF particle mass (compare to equation (15)) is

$$m = \frac{\hbar\omega_0}{c^2} \sqrt{\frac{2\delta t}{t_{\rm GW}}} \tag{31}$$

and the initial pulse duration is

$$\tau_0 = \frac{2}{\omega_0 \tau} \delta t \tag{32}$$

For a fixed total energy ΔE that is released into the ELF channel, the maximum field amplitude at the sensor is fixed to

$$\phi_{\text{max}} \approx \frac{1}{R} \left(\frac{c\Delta E}{2\pi^{3/2} \omega_0^2 \tau} \right)^{1/2} \tag{33}$$

where we take the amplitude for the Gaussian envelope (equation (29)) as a fiducial value.

We consider a variety of ELF production scenarios and leave the envelope of the arriving wave packet undefined. This uncertainty can be incorporated into a statistical analysis using the excess power statistic³³. This method is based on the time–frequency decomposition of the data and detects events based on their signature of having more power in a time–frequency interval than one expects from detector noise alone. Excess power is the optimal method for searching for events in situations for which only a rough idea of the frequency and duration of the signal is known^{13,34}.

Suppose the data streams from the sensors are sampled uniformly at a rate $1/\Delta_p$, which yields a time series **d** with elements $d_1, d_2, \ldots, d_j, \ldots, d_{N_{\text{tot}}}$ for a data set with N_{tot} points. Each data point $d_j = s_j + n_j$ comprises contributions from both the sought ELF signal s_i and intrinsic sensor noise n_i .

The discrete Fourier transform (DFT) in a sliding time window is used to partition the data stream into segments of time and frequency (tiles). Our goal is to quantify the power that is contained in each time-and-frequency tile of the data due to only noise, and thereby extract contributions due to putative ELF signals. To this end, the data stream can be split into two gross segments: before and after the electromagnetic or gravitational-wave triggers on detectors on Earth. The noise characteristics can be determined fully from the pre-trigger data, as during that period $d_j = n_j$ by our assumptions. We assume that the sensor noise is distributed as a Gaussian and is stationary, but we do not assume it is necessarily white (which, with appropriate filtering, is generally the case for the GNOME and GPS data^{5,35}). Below, we focus on a single sensor and later generalize to a network of sensors.

The time series **d** is partitioned into segments that contain N_w elements. N_w is chosen to be an even number for notational convenience. Each segment is associated with a data index w, which coincides with the midpoint of the partition: $w = N_w/2$, $3N_w/2$, $5N_w/2$, ... and a time $t_w = w\Delta_v$.

The Fourier amplitudes for each time partition are then given by

$$\tilde{d}_{p,w} = \sum_{j=w-N_w/2}^{w+N_w/2} d_{w-j} e^{2\pi i (w-j)p/N_w}$$
(34)

where the index p enumerates the DFT frequencies and $f_p = p/(N_w \Delta_t)$ ranges from zero to the Nyquist frequency $1/(2\Delta_t)$. The zero-frequency component ($f_p = 0$) and Nyquist frequency amplitudes can be removed from the analysis because their statistical properties differ from that of the rest of the amplitudes (for example, see refs. 36,37). This simplification does not alter the conclusions. Equation (34) represents a two-dimensional discrete map of complex time–frequency values. The frequency and time indices reference individual tiles (p, w) in such a map.

Using the pre-event data ($d_k \equiv n_k$), we determine the (two-sided) power spectral density (PSD) of the sensor noise

$$\tilde{C}_{p} \equiv \langle \tilde{n}_{p} (\tilde{n}_{p})^{*} \rangle \tag{35}$$

where the average is taken over multiple pre-event time windows. The post-event data PSD is normalized to the noise PSD

$$\mathcal{E}_{p,w} \equiv \frac{|\tilde{d}_{p,w}|^2}{\tilde{C}_p} \tag{36}$$

The quantities $\mathcal{E}_{p,w}$ quantify the excess power in the (p, w) tile. (Note that our definition of excess power is larger by a factor of 2 compared to that in ref. ³³.) In the absence of the sought-after ELF signal, $\langle \mathcal{E}_{p,w} \rangle = 1$. A time–frequency decomposition map for a Gaussian ELF wave packet (equation (29)) is shown in Fig. 2.

We adopt the method of ref. ³³ to incorporate our knowledge about the expected ELF signals. In that work, the search method probes all of the tiles that occupy a rectangular area in the time–frequency decomposition map. Here, we restrict the probed tiles to the areas that are spanned by the expected ELF signals. Indeed, the expected ELF signal with the fixed parameters $(\delta t, \tau, \omega_0)$ contains substantial power in only a subset of tiles (Fig. 2 and Supplementary Fig. 2). Thereby, we define the excess power statistic \mathcal{E}_{ELF} by the summation over the tiles that contain ELFs

$$\mathcal{E} = \sum_{(p,w) \in \text{ELF}} \mathcal{E}_{p,w} \tag{37}$$

In the absence of noise in the post-event data, the total excess power contained in the ELF signal is

$$\mathcal{E}_{\text{ELF}} = \sum_{(p,w)\in\text{ELF}} \frac{\left|\tilde{s}_{p,w}\right|^2}{\tilde{C}_p} \tag{38}$$

The probability distribution function for the statistic \mathcal{E} is 38

$$p_{M}(\mathcal{E}|\mathcal{E}_{\text{ELF}}) = I_{M-1} \left(2\sqrt{\mathcal{E}\mathcal{E}_{\text{ELF}}}\right) \left(\sqrt{\frac{\mathcal{E}}{\mathcal{E}_{\text{ELF}}}}\right)^{M-1} e^{-(\mathcal{E}+\mathcal{E}_{\text{ELF}})}$$
(39)

where $I_{M-1}(\cdots)$ is the modified Bessel function, and M is the total number of tiles that contain ELFs. This distribution can be recognized, up to a change of scale, as a noncentral χ^2 distribution with 2M degrees of freedom. The mean and variance are given by

$$\left\langle \mathcal{E}\right\rangle = M + \mathcal{E}_{ELF}, \quad Var\left(\mathcal{E}\right) = M + 2\mathcal{E}_{ELF} \tag{40} \label{eq:elliptic_energy}$$

Next, we would like to establish the detector discovery reach for \mathcal{E}_{ELF} at the 95% confidence level. To this end, we compute the upper tail probability threshold given the observed value \mathcal{E}_{obs} of the statistic (equation (38), the observed value is computed with sensor data)

$$\int_{\mathcal{E}_{ab}}^{\infty} p_M(\mathcal{E}|\mathcal{E}_{ELF}^{95\%}) \, d\mathcal{E} = 0.95$$
 (41)

This is an implicit equation for the detectable ELF signal power $\mathcal{E}_{\text{ELF}}^{95\%}$. Equation (41) can be represented in terms of the Marcum Q function, which is a part of standard mathematical libraries,

$$Q_{\rm M}\left(\sqrt{2\mathcal{E}_{\rm ELF}^{95\%}},\sqrt{2\mathcal{E}_{\rm obs}}\right) = 0.95 \tag{42}$$

To find the sensitivity to ELFs, we assume that the ELF signal is well below the noise floor. Then, in equation (42), $\mathcal{E}_{\text{obs}} \approx M$ (see equation (40)). We invert the resulting equation in the limit of $M \gg 1$ and find

$$\mathcal{E}_{\text{ELF}}^{95\%} \approx 1.7\sqrt{M}$$
 (43)

This result is consistent with qualitative signal-to-noise ratio arguments. The signal-to-noise ratio (SNR) can be defined as

$$SNR = \frac{\mathcal{E}_{ELF}}{\sqrt{Var\left(\mathcal{E}\right)}} = \frac{\mathcal{E}_{ELF}}{\sqrt{M}}$$

where we use equation (40) for the variance with only the noise contribution. Holding constant the signal-to-noise ratio value results in the same \sqrt{M} scaling of the minimum detectable ELF power as in the more rigorous estimate (equation (43)).

With these results, we can determine the sensitivity of a sensor to coupling constants that characterize ELF portals. We parameterize the ELF-induced signals in the sensor as

$$s(t) = \begin{cases} \gamma_1 C_1 \phi(t) , & \text{linear} \\ \gamma_2 C_2 \phi(t)^2 , & \text{quadratic} \end{cases}$$
(44)

Here, γ_1 and γ_2 are the coupling constants to be constrained and C_i are known constants that are determined by the particular sensor.

Next, we compute \mathcal{E}_{ELF} , the excess power statistic (equation (38)) for the ELF signals (equation (44)). The signal powers are normalized to the noise PSD \tilde{C}_{ν} . For a sensor that exhibits white noise of variance σ^2 , the noise PSD is $\tilde{C}_p = N_w \sigma^2$ and

$$\mathcal{E}_{\text{ELF}} = \frac{1}{N_w \sigma^2} \sum_{(p,w) \in \text{ELF}} |\tilde{\mathbf{s}}_{p,w}|^2 \tag{45}$$

The sum over ELF contributions can be simply evaluated in the limit when the temporal window size T_w is much smaller than duration of the ELF burst τ . In this case, we can neglect the time variation in the ELF envelope over the window. In the window, the ELF frequencies span the frequency interval $|d\omega/dt|T_w = T_w/(\tau \tau_0)$, where the slope is given by equation (27). Without loss of generality, we require that this spanned frequency interval is smaller than the DFT frequency resolution Δ_m = $2\pi/T_{w}$. We require also that adjacent windows map instantaneous ELF frequencies to distinct and adjacent DFT frequencies. Under these assumptions, the total number M of tiles that contain ELF signals and the 'optimal' window duration T_{w}

$$M \approx \tau / T_{\rm w}$$
 (46)

$$T_{\rm w} \approx \sqrt{2\pi\tau\tau_0}$$
 (47)

With the negligible ELF frequency variation over the window, the field PSD is

$$|\tilde{\phi}_{w,p}|^2 \approx \frac{1}{4} |\phi_{\text{env}}(t_w)|^2 N_w^2 \delta_{p,p_0}$$
 (48)

where $\phi_{env}(t_w)$ is the value of the ELF burst envelope in the window and p_0 corresponds to the DFT frequency that is nearest to the ELF frequency in the window. We sum over windows and arrive at the minimal detectable ELF power

$$\mathcal{E}_{\text{ELF},1} \approx \frac{\sqrt{\pi}}{4} \gamma_1^2 C_1^2 \frac{1}{\sigma^2} \frac{\tau}{\Delta_t} \phi_{\text{max}}^2 \tag{49}$$

for the linear portal. To arrive at this result, we evaluate the sum in the continuous limit.

$$\begin{array}{l} \sum_{(p,w) \in \mathrm{ELF}} |\tilde{\phi}_{p,w}|^2 \approx \frac{N_w^2}{4} \sum_{w \in \mathrm{ELF}} |\phi_{\mathrm{env}}(t_w)|^2 \\ \approx \frac{N_w^2}{4T_w} \int_{-\infty}^{\infty} \phi_{\mathrm{env}}^2(t) \, \mathrm{d}t \end{array}$$

and use the envelope for the Gaussian pulse. A similar evaluation for a quadratic portal leads to

$$\mathcal{E}_{\text{ELF},2} \approx \sqrt{\frac{\pi}{2}} \gamma_2^2 C_2^2 \frac{1}{16\sigma^2} \frac{\tau}{\Lambda_t} \phi_{\text{max}}^4$$
 (50)

Notice that for the quadratic coupling,

$$\begin{split} \cos^2\!\left(\omega_0(t-t_\mathrm{s}) - \! \textstyle\frac{1}{2\tau\tau_0}(t-t_\mathrm{s})^2\right) &= \\ \textstyle\frac{1}{2}\left[1 + \cos\!\left(2\omega_0(t-t_\mathrm{s}) - \! \textstyle\frac{1}{\tau_0\tau}(t-t_\mathrm{s})^2\right)\right] \end{split}$$

that is, the central frequency and the slope are doubled, but the field amplitude is reduced effectively by $\sqrt{2}$. We ignore the zero-frequency contribution in our present approach, although it can serve as an additional signature for the quadratic interactions.

In equations (49) and (50), the ratio τ/Δ_t can be recognized as the total number of sampled points during the ELF pulse duration. These formulae, together with the minimum detectable excess power (equation (43)), yield the constraint on the coupling constant

$$\gamma_1^{95\%} \approx 2 \frac{\sigma}{\mathcal{C}_1 \phi_{\text{max}}} \sqrt{\frac{\Delta_t}{\tau}} \left(\frac{\tau}{\tau_0}\right)^{1/8} \tag{51}$$

for the linear coupling and

$$\gamma_2^{95\%} \approx 4 \frac{\sigma}{\mathcal{C}_2 \phi_{\max}^2} \sqrt{\frac{\Delta_t}{\tau}} \left(\frac{\tau}{\tau_0}\right)^{1/8} \tag{52}$$

for the quadratic coupling. Here, we use the total number of tiles that contain ELFs (equation (46)) and the optimal window size (equation (47)). As the ELF signal is coherent across a sensor network, the above constraints are improved by $\sqrt{N_s}$ for a network of N_s sensors (see more detailed discussions of the statistical analysis for sensor networks in refs. 36,37,39). The dependence on the ratio τ/τ_0 in equation (52) is weak, and we drop this dependence. Then, with the maximum field amplitude (equation(33)),

$$\gamma_1^{95\%} \approx 5 \frac{\sigma}{C_1 \sqrt{N_s}} R\omega_0 \sqrt{\frac{\Delta_t}{c\Delta E}}$$
 (53)

$$\gamma_2^{95\%} \approx 40 \frac{\sigma}{C_2 \sqrt{N_s}} \frac{R^2 \omega_0^2}{c \Delta E} \sqrt{\Delta_t \tau}$$
 (54)

These constraints depend on the ELF central frequency ω_0 . The derivations shown in the second section of the Methods are valid in the limit $\omega_0 \gg \Delta \omega = 1/\tau_0$. To avoid DFT aliasing, it is sufficient to require that $\omega_0 \ll \pi/\Delta_i$; that is, ω_0 is well below the Nyquist frequency. Explicitly,

$$1/\tau_0 \ll \omega_0 \ll \pi/\Delta_t \tag{55}$$

Although the upper limit of equation (55) is fixed by the sensor sampling rate, the initial ELF pulse duration τ_0 depends on production mechanisms. For a general search with τ_0 as a free parameter, the minimum detectable ELF frequency is on the order of the DFT (angular) frequency resolution, $2\pi/T_{w}$. Given that the typical rate of LIGO gravitational-wave detections is a few events per year, we adopt $T_{\rm w} \lesssim 10^6$ s, which leads to $(\omega_0)_{\rm min} \approx (2\pi) \times 10^{-6}\,$ Hz.

Atomic clocks and cavities. Atomic clocks compare the frequency of an atomic transition with the resonance frequency of a local oscillator, typically a reference optical or microwave cavity. The atoms are interrogated with laser or microwave pulses that are outcoupled from the cavities, whose frequency is kept in resonance with the atomic transition by a feedback loop. The typical interrogation time t_0 for a modern atomic clock is on the order of a second. Therefore, the atomic clocks essentially measure the quantum phase Φ of an atomic oscillator with respect to the local oscillator. Our analysis will hold in the limit when the period of the ELF oscillations is larger than the interrogation time; that is, $1/\omega_0 \gg t_0$.

As both the atomic oscillator and the local oscillator can be affected by the ELFs, the ELF-induced accumulated phase difference is

$$\Phi_{j}^{\text{ELF}} = 2\pi \int_{t_{j-1}}^{t_{j}} [\nu_{\text{atom}}^{\text{ELF}}(t') - \nu_{\text{LO}}^{\text{ELF}}(t')] dt'
\approx 2\pi [\nu_{\text{atom}}^{\text{ELF}}(t_{j}) - \nu_{\text{LO}}^{\text{ELF}}(t_{j})] t_{0}$$
(56)

given that the observable ELF oscillations are slow over the interrogation time. The frequency difference that results is typically recorded, and therefore, we consider a time series of fractional frequency excursions

$$s_j \equiv \frac{\nu_{\text{atom}}(t_j) - \nu_{\text{LO}}(t_j)}{\nu_{\text{clock}}} \tag{57}$$

taken at $t_i = jt_0$; $j = 1, 2, ..., N_{tot}$, with the unperturbed clock frequency ν_{clock} . Atomic and cavity frequencies can be affected by varying fundamental constants, such as the fine-structure constant $\alpha = e^2/\hbar c$ and/or fermion masses m_e We consider a model in which an ELF drives such variations as described by the following phenomenological Lagrangians (portals) that couple standard model fields and ELFs

$$\mathcal{L}_{\text{clock}}^{(1)} = \left(-\sum_{f} \Gamma_{f}^{(1)} m_{f} c^{2} \overline{\psi}_{f} \psi_{f} + \frac{\Gamma_{\alpha}^{(1)}}{4} F_{\mu\nu}^{2}\right) \sqrt{\hbar c} \ \phi \tag{58}$$

$$\mathcal{L}_{\rm clock}^{(2)} = \left(-\sum_{f} \Gamma_{f}^{(2)} m_{f} c^{2} \bar{\psi}_{f} \psi_{f} + \frac{\Gamma_{\alpha}^{(2)}}{4} F_{\mu\nu}^{2}\right) \hbar c \ \phi^{2} \tag{59}$$

 $\mathcal{L}_{\text{int}}^{(1)}$ is linear in the exotic field ϕ , and $\mathcal{L}_{\text{int}}^{(2)}$ is quadratic. The structure of these portals is such that various parts of the standard model Lagrangian are multiplied by exotic fields, in which the Γ terms are the associated coupling constants that are to be determined or constrained. In the above interactions, f runs over all of the standard model fermions (fields ψ_t and masses m_t), and F_{uu} is the Faraday tensor; gluon, Higgs or weak-interaction contributions may be included, if desired. We refer the interested reader to the discussion of

the technical naturalness of such Lagrangians in ref. 7 . In these expressions, the combination $\sqrt{\hbar c}$ ϕ is measured in units of energy, [E]. Then, $\Gamma_{X}^{(1)}$ are measured in units of $[E]^{-1}$ and $\Gamma_{X}^{(2)}$ in $[E]^{-2}$.

The portals (equations (58) and (59)) lead to the effective redefinition of fermion masses and the fine-structure constants:

$$m_{f}(\mathbf{r},t) = m_{f} \times \left[1 + \Gamma_{f}^{(n)} \left(\sqrt{\hbar c} \phi(\mathbf{r},t) \right)^{n} \right]$$

$$\alpha(\mathbf{r},t) \approx \alpha \times \left[1 + \Gamma_{\alpha}^{(n)} \left(\sqrt{\hbar c} \phi(\mathbf{r},t) \right)^{n} \right]$$
(60)

for the linear (n=1) and quadratic (n=2) portals, where m_f and α are the nominal (unperturbed) values.

Atomic frequencies are affected primarily by the induced variation of the Rydberg constant, $\mathcal{R}_{\infty}=m_{\rm e}c^2\alpha^2$. Optical clocks can exhibit an additional dependence on α owing to relativistic effects. Microwave clocks operate on hyperfine transitions and hence are affected by the variation in the quark masses m_q and the strong coupling constant. In addition, the variation in the Bohr radius $a_0=\alpha^{-1}h/(m_ec)$ affects the cavity length $L\propto a_0$ and therefore the cavity resonance frequencies. Conventionally, coefficients $\kappa_X=\partial \ln \nu/\partial \ln X$ that quantify the sensitivity of a resonance frequency ν are introduced to the variation in the fundamental constant X. Then,

$$\begin{array}{ll} \kappa_{m_e}^{\rm atom} \approx 1, & \kappa_{\alpha}^{\rm atom} \approx 2, \\ \kappa_{m_e}^{\rm cavity} \approx -1, & \kappa_{\alpha}^{\rm cavity} \approx -1. \end{array}$$

It is worth noting that there are exceptional cases of enhanced sensitivity to the variation of fundamental constants; for example, in the actively pursued, but yet not demonstrated, ^{229}Th nuclear clock*10 ($\kappa_{\alpha}\approx 10^4$, ref. 41), and in clocks based on highly charged ions*2 ($\kappa_{\alpha}\lesssim 10^2$, ref. 43). The above arguments presuppose an instantaneous adjustment of the resonance or transition frequencies to the variation of fundamental constants*50.

In terms of the differential sensitivity coefficient $K_X = \kappa_X^{\rm atom} - \kappa_X^{\rm LO}$ and the effective coupling constant

$$\Gamma_{\text{eff}}^{(n)} \equiv \sum_{X} K_X \Gamma_X^{(n)} \tag{61}$$

we can write the sought ELF signal (equation (57)) as

$$s_{j} = \Gamma_{\text{eff}}^{(n)} \left(\sqrt{\hbar c} \phi(t_{j}) \right)^{n} \tag{62}$$

where n = 1, 2 indicates the linear and quadratic portals, respectively.

Owing to the relatively low, ~Hz, sampling rate of atomic clocks, a terrestrial network of atomic clocks would not be able to track the propagation of the ultrarelativistic ELF pulse through the network, as discussed in the main text. However, optical cavities can have much faster, ≥10 kHz, sampling rates. A network that comprises multiple cavities was proposed in the context of the search for ultralight dark matter²³, and we believe that such a network can be adopted for ELF searches, as well. In essence, each node in the network would contain two distinct cavities: one with a rigid spacer and the other with suspended mirrors (without the spacer, similar to LIGO cavities). The resonance frequency of the cavity with a rigid spacer is affected by the variation of fundamental constants, but that of the cavity without the spacer is not. In which case, the experiment would involve a comparison of these resonance frequencies.

The comparison of equation (62) with our generic ELF signal template (equation (44)) leads to the identification $\gamma_n = \Gamma_{\rm eff}^{(n)}$ and $\mathcal{C}_n = (\hbar c)^{n/2}$. To apply the derived constraints (equations (53) and (54)), we need also to make an assumption about the nature of the measurement noise, which for atomic clocks is characterized by the Allan deviation $\sigma_y(\tau_{\rm meas})$, where $\tau_{\rm meas}$ is the measurement time. If the Allan deviation scales as $\sigma_y(\tau_{\rm meas}) \propto 1/\sqrt{\tau_{\rm meas}}$, the measurement noise is dominated by the white frequency noise. Then, in the constraint equations (53) and (54), $\sigma = \sigma_y(t_0) = \sigma_y(\Delta_t)$, and using the methods described in the Supplementary Information, we arrive at constraints on the effective coupling constants (at the 95% confidence level)

$$\Gamma_{\text{eff}}^{(1)} \lesssim 5 \frac{\sigma_y(\Delta_t)}{\sqrt{N_s}} \left(\frac{\omega_0}{c} R\right) \left(\frac{\Delta_t}{\hbar \Delta E}\right)^{1/2}$$
 (63)

$$\Gamma_{\text{eff}}^{(2)} \lesssim 40 \frac{\sigma_y(\Delta_t)}{\sqrt{N_s}} \left(\frac{\omega_0}{c}R\right)^2 \frac{1}{\Delta E} \left(\frac{\Delta_t \tau}{\hbar^2}\right)^{1/2} \tag{64}$$

In Supplementary Table 1, we report the estimated sensitivity of existing and future clock networks.

Optical cavities. The constraint equations (53) and (54) apply immediately with $\Gamma_{\rm eff}^{(n)}$ (equation (61)) and involve the sensitivity coefficient of the rigid spacer cavity: $K_X = \kappa_X^{\rm cavity}$. Another possible detector with a similar high sampling rate is the three-arm Mach–Zender interferometer¹⁴, in which the delays of the laser pulse are compared while they travel through an optical cavity and an optical fibre.

Linear couplings. Here, we focus on the linear coupling and assume for simplicity that one of the couplings dominates; for example, $\Gamma_{\rm eff}^{(1)} \approx K_\alpha \Gamma_\alpha^{(1)}$. This assumption is hardly necessary, but it clarifies the role of the sensitivity coefficients K_X . We recast the constraint equation (63) in terms of moduli 45 $d_X \equiv (E_{\rm Pl}/\sqrt{4\pi})\Gamma_X^{(1)}$, in which $E_{\rm Pl} = \sqrt{\hbar c^5/G}$ is the Planck energy

$$d_X \lesssim \frac{E_{\rm Pl} \, \sigma_y(\Delta_t)}{K_X \, \sqrt{N_{\rm s}}} \left(\frac{\omega_0}{c} \, R\right) \left(\frac{\Delta_t}{\hbar \Delta E}\right)^{1/2} \tag{65}$$

or, in practical units,

$$d_X \lesssim 40 \frac{1}{K_X \sqrt{N_s}} \left(\frac{\sigma_y(\Delta_t)}{10^{-16}} \right) \left(\frac{\omega_0}{2\pi \text{ Hz}} \right) \left(\frac{R}{\text{Mpc}} \right) \left(\frac{\Delta_t}{\text{s}} \right)^{1/2} \left(\frac{\Delta E}{M_{\odot} c^2} \right)^{-1/2}$$
(66)

Here, as the reference value for the Allan deviation, we take $\sigma_y(1 \text{ s}) \approx 10^{-16}$, which is characteristic of modern optical lattice clocks⁶.

We focus on the electron mass modulus d_{m_e} and the electromagnetic gauge modulus d_e ($X=\alpha$ in this case). The most stringent limits on these moduli come from tests for violation of the equivalence principle (see Fig. 1 of ref. ⁴⁵). For the parameter space that is relevant to clocks and cavities, the excluded regions are $d_e \gtrsim 10^{-3}$ and $d_{m_e} \gtrsim 10^{-2}$.

Quadratic couplings. For consistency with prior literature, we rewrite the constraint equation (64) in terms of the energy scale $\Lambda_X = 1/\sqrt{|\Gamma_X^{(2)}|}$,

$$\Lambda_X \gtrsim 0.2 \sqrt{|K_X|} \left(\frac{\sqrt{N_s}}{\sigma_y(\Delta_t)}\right)^{1/2} \left(\frac{c}{R\omega_0}\right) \Delta E^{1/2} \left(\frac{\hbar^2}{\Delta_t \tau}\right)^{1/4}$$

Here, we assume that the variation in a fundamental constant X dominates (for example, $\Gamma_{eff}^{(2)} \approx K_{m_e} \Gamma_{m}^{(2)}$). In practical units,

$$\frac{\Delta_{X}}{\text{TeV}} \gtrsim 2 \times 10^{5} |K_{X}|^{1/2} N_{s}^{1/4} \left(\frac{\sigma_{y}(\Delta_{t})}{10^{-16}} \right)^{-1/2} \times \left(\frac{R}{\text{Mpc}} \times \frac{\omega_{0}}{2\pi \text{ Hz}} \right)^{-1} \left(\frac{\Delta E}{M_{\odot}c^{2}} \right)^{1/2} \left(\frac{\Delta_{t}}{1 \text{ s}} \times \frac{\tau}{10^{2} \text{ s}} \right)^{-1/4}$$
(67)

The most stringent constraints on the energy scales

$$\Lambda_{m_e,\alpha} \gtrsim 3 \text{ TeV}$$
 and $\Lambda_{m_p} \gtrsim 10 \text{ TeV}$ (68)

come from the bounds on the thermal emission rate from the cores of supernovae²⁶. The authors of ref. ²⁶ analysed the emissivity of ϕ quanta due to pair annihilation of photons and other processes, such as bremsstrahlung-like emission. They also considered tests of the gravitational force that result in similar constraints; compared to linear Lagrangians, these constraints are mild, because the quadratic Lagrangians lead to the interaction potentials that scale as an inverse cube of the distance, as only the exchange of pairs of ϕ 's are allowed (for linear Lagrangians, the ϕ -mediated interaction potentials scale as the inverse distance). Black-hole superradiance additionally excludes certain narrow mass regions⁴⁶. The enumerated constraints do not depend on the assumption that ELFs are the dominant fraction of dark matter. If ELFs do contribute to dark matter, see ref. ⁴⁶ for additional constraints, such as those from Big Bang nucleosynthesis.

From the numerical pre-factor in equation (67), it is clear that a generic ELF search would probe energy scales well beyond the existing astrophysical and gravity test bounds (Fig. 3).

Magnetometers. Atomic magnetometers, such as those employed in GNOME⁵, are sensitive to spin-dependent energy shifts. We consider interaction Lagrangians⁴ that are linear, $\mathcal{L}^{(1)}$, and quadratic, $\mathcal{L}^{(2)}$, in the spin-0 ELFs ϕ ,

$$\mathcal{L}_{\text{mag}}^{(1)} = f_l^{-1} J^{\mu} \partial_{\mu} \phi \tag{69}$$

$$\mathcal{L}_{\text{mag}}^{(2)} = f_q^{-2} J^\mu \partial_\mu \phi^2 \tag{70}$$

In these expressions, $J^{\mu}=\bar{\psi}\gamma^{\mu}\gamma_{5}\psi$ is the axial-vector current for standard model fermions, and f_{l} and f_{q} are the characteristic energy scales that are associated with the linear and quadratic spin portals, respectively. The relevant contribution to the Dirac Hamiltonian can be computed as

$$H_{\rm int}\psi = -\gamma_0 \left[\frac{\partial \mathcal{L}_{\rm int}}{\partial \bar{\psi}} - \partial_\mu \left(\frac{\partial \mathcal{L}_{\rm int}}{\partial (\partial_\mu \bar{\psi})} \right) \right] \tag{71}$$

which leads to

$$H_{\text{mag}}^{(1)} = -\frac{1}{f_{*}} \left(\gamma_{5} \frac{\partial}{\partial t} \phi + \Sigma \cdot \nabla \phi \right) \tag{72}$$

$$H_{\rm mag}^{(2)} = -\frac{1}{f_q^2} \left(\gamma_5 \frac{\partial}{\partial t} \phi^2 + \mathbf{\Sigma} \cdot \nabla \phi^2 \right) \tag{73}$$

LETTERS NATURE ASTRONOMY

Here, we use the identities $\gamma_0 \gamma_0 = 1$ and $\gamma_0 \gamma^i \gamma_5 = \Sigma^i$ with the spin matrix

$$\Sigma = \begin{pmatrix} \sigma & 0 \\ 0 & \sigma \end{pmatrix} \tag{74}$$

We compute the expectation value of these Hamiltonians and obtain the effective spin-dependent interactions, $\,$

$$H_{\text{mag}}^{(1)} \approx -\frac{2(\hbar c)^{3/2}}{f_I} \mathbf{S} \cdot \nabla \phi \tag{75}$$

$$H_{\text{mag}}^{(2)} \approx -\frac{2(\hbar c)^2}{f_a^2} \mathbf{S} \cdot \nabla \phi^2 \tag{76}$$

which are equivalent to the nonrelativistic Hamiltonians that are often seen in the literature (for example, ref. 2). The terms that contain time derivatives of the ϕ field are neglected in the nonrelativistic limit for atomic electrons or nucleons, as the γ_5 matrix mixes large and small components of the Dirac bi-spinors. S is the atomic or nuclear spin.

The ELF Hamiltonians that are described by equations (75) and (76) can be related to the general forms of the ELF interactions given in equation (44) through the following identifications: $\gamma_1=-\frac{1}{f_1}$, $C_1\approx 2\hbar^{3/2}c^{1/2}\omega_0$, $\gamma_2=-\frac{1}{f_3^2}$, $C_2\approx 4\hbar^2c\omega_0$, where we have kept only the leading terms when taking the gradients of ϕ and ϕ^2 . Note that the atomic and nuclear structure $^{e\gamma}$, as well as geometrical considerations 5 , must be taken into account to interpret magnetometer data in terms of couplings to ELFs, but for the rough estimates presented in this work, we ignore these details. With these identifications, from equations (53) and (54) and with details found in the Supplementary Information, we arrive at the constraints on the effective coupling constants at the 95% confidence level:

$$f_l \gtrsim 0.4 \ \hbar^{3/2} c \frac{\sqrt{N_s}}{\sigma_m(\Delta_t)\sqrt{\Delta_t}} \frac{\sqrt{\Delta E}}{R}$$
 (77)

$$f_q^2 \gtrsim 0.1 \ \hbar^2 c^2 \frac{\sqrt{N_s}}{\sigma_m(\Delta_t)\sqrt{\Delta_t \tau}} \frac{\Delta E}{R^2 \omega_0} \tag{78}$$

Here, $\sigma_m(\Delta_t)$ is the magnetometer energy resolution. A typical GNOME magnetometer has a bandwidth of ~100 Hz and, integrating over a time Δ_p can measure the magnetic field with a precision given by $\delta B \approx 100~{\rm fT}\sqrt{\rm s}/\sqrt{\Delta_t}$. Therefore,

$$\sigma_m(\Delta_t) \approx g\mu_{\rm B}\delta B \approx \frac{10^{-18}}{\sqrt{\Delta_t}} {\rm eV}\sqrt{\rm s}$$
 (79)

where g is the Lande factor (which depends on the atomic species used in the magnetometer) and $\mu_{\rm B}$ is the Bohr magneton. The prior astrophysical limits on energy scales are^{4,48} $f_{\rm i} \gtrsim 2 \times 10^8$ GeV and $f_q \gtrsim 10^4$ GeV. In Supplementary Table 2, we report the estimated sensitivity of existing and future magnetometer networks.

Data availability

The data that support the plots within this paper and other findings of this study are available from the corresponding author upon reasonable request.

Received: 10 February 2020; Accepted: 24 September 2020; Published online: 02 November 2020

References

- Abbott, B. P. et al. Multi-messenger observations of a binary neutron star merger. Astrophys. J. Lett. 848, L12 (2017).
- Mod. Phys. 90, 025008 (2018).Budker, D. & Jackson Kimball, D. F. (eds) Optical Magnetometry (Cambridge

Safronova, M. S. et al. Search for new physics with atoms and molecules. Rev.

- Budker, D. & Jackson Kimball, D. F. (eds) Optical Magnetometry (Cambridge Univ. Press, 2013).
- Pospelov, M. et al. Detecting domain walls of axionlike models using terrestrial experiments. Phys. Rev. Lett. 110, 021803 (2013).
- Afach, S. et al. Characterization of the global network of optical magnetometers to search for exotic physics (GNOME). *Phys. Dark Universe* 22, 162180 (2018).
- Ludlow, A. D., Boyd, M. M., Ye, J., Peik, E. & Schmidt, P. O. Optical atomic clocks. Rev. Mod. Phys. 87, 637 (2015).
- Derevianko, A. & Pospelov, M. Hunting for topological dark matter with atomic clocks. Nat. Phys. 10, 933–936 (2014).
- Roberts, B. M. et al. Search for domain wall dark matter with atomic clocks on board global positioning system satellites. *Nat. Commun.* 8, 1195 (2017).
- 9. Baumann, D., Chia, H. S. & Porto, R. A. Probing ultralight bosons with binary black holes. *Phys. Rev. D* **99**, 044001 (2019).

- Raffelt, G. G. Particle physics from stars. Annu. Rev. Nucl. Part. Sci. 49, 163–216 (1999).
- Tkachev, I. I. Fast radio bursts and axion miniclusters. JETP Lett. 101, 1–6 (2015).
- Loeb, A. Lets talk about black hole singularities. Preprint at https://arxiv.org/ abs/1805.05865 (2018).
- Arvanitaki, A., Baryakhtar, M., Dimopoulos, S., Dubovsky, S. & Lasenby, R. Black hole mergers and the QCD axion at Advanced LIGO. *Phys. Rev. D* 95, 043001 (2017).
- Baryakhtar, M., Lasenby, R. & Teo, M. Black hole superradiance signatures of ultralight vectors. *Phys. Rev. D* 96, 035019 (2017).
- Fujii, Y. & Maeda, K. The Scalar-Tensor Theory of Gravitation (Cambridge Univ. Press, 2007).
- Franciolini, G., Hui, L., Penco, R., Santoni, L. & Trincherini, E. Effective field theory of black hole quasinormal modes in scalar–tensor theories. *J. High Energy Phys.* 2019, 127 (2019).
- Barausse, E., Palenzuela, C., Ponce, M. & Lehner, L. Neutron-star mergers in scalar-tensor theories of gravity. Phys. Rev. D 87, 081506 (2013).
- Krause, D. E., Kloor, H. T. & Fischbach, E. Multipole radiation from massive fields: application to binary pulsar systems. *Phys. Rev. D* 49, 6892–6906 (1994).
- Abbott, B. P. et al. Observation of gravitational waves from a binary black hole merger. *Phys. Rev. Lett.* 116, 061102 (2016).
- Abbott, B. P. et al. GW170814: a three-detector observation of gravitational waves from a binary black hole coalescence. *Phys. Rev. Lett.* 119, 141101 (2017).
- Abbott, B. P. et al. GW170817: observation of gravitational waves from a binary neutron star inspiral. *Phys. Rev. Lett.* 119, 161101 (2017).
- Jackson Kimball, D. F. et al. Searching for axion stars and Q-balls with a terrestrial magnetometer network. *Phys. Rev. D* 97, 043002 (2018).
- Geraci, A. A., Bradley, C., Gao, D., Weinstein, J. & Derevianko, A. Searching for ultralight dark matter with optical cavities. *Phys. Rev. Lett.* 123, 31304 (2019).
- Cronin, A. D., Schmiedmayer, J. & Pritchard, D. E. Optics and interferometry with atoms and molecules. Rev. Mod. Phys. 81, 1051 (2009).
- Geraci, A. A. & Derevianko, A. Sensitivity of atom interferometry to ultralight scalar field dark matter. Phys. Rev. Lett. 117, 261301 (2016).
- Olive, K. A. & Pospelov, M. Environmental dependence of masses and coupling constants. *Phys. Rev. D* 77, 043524 (2008).
- Roberts, B. M. et al. Search for transient variations of the fine structure constant and dark matter using fiber-linked optical atomic clocks. *New J. Phys.* 22, 093010 (2020).
- Paul, D. Binary neutron star merger rate via the luminosity function of short gamma-ray bursts. Mon. Not. R. Astron. Soc. 477, 4275–4284 (2018).
- Tino, G. M. et al. SAGE: a proposal for a space atomic gravity explorer. Eur. Phys. I. D 73, 228 (2019).
- Peskin, M. E. & Schroeder, D. V. An Introduction to Quantum Field Theory (Perseus Books, 1995).
- Abbott, B. P. et al. GW170608: observation of a 19 solar-mass binary black hole coalescence. Astrophys. J. Lett. 851, L35 (2017).
- 32. Jackson, J. D. Classical Electrodynamics 3rd edn (John Wiley, 1999).
- 33. Anderson, W. G. et al. Excess power statistic for detection of burst sources of gravitational radiation. *Phys. Rev. D* **63**, 042003 (2001).
- 34. Maggiore, M. Gravitational Waves. Volume 1: Theory and Experiments (Oxford Univ. Press, 2008).
- Roberts, B. M. et al. Search for domain wall dark matter with atomic clocks on board global positioning system satellites. *Nat. Commun.* 8, 1195 (2017).
- Derevianko, A. Detecting dark-matter waves with a network of precision-measurement tools. Phys. Rev. A 97, 042506 (2018).
- Romano, J. D. & Cornish, N. J. Detection methods for stochastic gravitational-wave backgrounds: a unified treatment. *Living Rev. Relativ.* 20, 2 (2017).
- Groth, E. J. Probability distributions related to power spectra. Astrophys. J. Suppl. Ser. 29, 285–302 (1975).
- Panelli, G., Roberts, B. M. & Derevianko, A. Applying matched-filter technique to the search for dark matter transients with networks of quantum sensors. EPJ Quantum Technol. 7, 5 (2020).
- Campbell, C. J. et al. Single-ion nuclear clock for metrology at the 19th decimal place. *Phys. Rev. Lett.* 108, 120802 (2012).
- Litvinova, E., Feldmeier, H., Dobaczewski, J. & Flambaum, V. Nuclear structure of lowest ²²⁹Th states and time-dependent fundamental constants. *Phys. Rev. C* 79, 064303 (2009).
- Dérevianko, A., Dzuba, V. A. & Flambaum, V. V. Highly charged ions as a basis of optical atomic clockwork of exceptional accuracy. *Phys. Rev. Lett.* 109, 180801 (2012).
- Dzuba, V. A. & Flambaum, V. V. Highly charged ions for atomic clocks and search for variation of the fine structure constant. *Hyperfine Interact.* 236, 7986 (2015).
- Savalle, E. et al. Novel approaches to dark-matter detection using space-time separated clocks. Preprint at https://arxiv.org/abs/1902.07192 (2019).

- Arvanitaki, A., Dimopoulos, S. & Van Tilburg, K. Sound of dark matter: searching for light scalars with resonant-mass detectors. *Phys. Rev. Lett.* 116, 031102 (2016).
- Sibiryakov, S., Sørensen, P. & Yu, T. -T. BBN constraints on universally-coupled ultralight scalar dark matter. Preprint at https://arxiv.org/ abs/2006.04820 (2020).
- Jackson Kimball, D. F. Nuclear spin content and constraints on exotic spin-dependent couplings. New J. Phys. 17, 073008 (2015).
- Chang, J. H., Essig, R. & McDermott, S. D. Supernova 1987A constraints on sub-GeV dark sectors, millicharged particles, the QCD axion, and an axion-like particle. J. High Energy Phys. 2018, 51 (2018).

Acknowledgements

We thank L. Bernard, G. Blewitt, S. Bonazzola, D. Budker, A. Furniss, S. Gardner, E. Gourgoulhon, K. Grimm, J. E. Lawler, R. Plotkin, M. Pospelov, J. Pradler, B. Safdi, A. P. Sen, J. E. Stalnaker and C. Will for discussions. This work was supported in part by the European Research Council under the European Unions Horizon 2020 research and innovation programme (grant no. 695405), the DFG Reinhart Koselleck project, the Polish National Science Centre (grant no. 2015/19/B/ST2/02129), the Simons and Heising-Simons Foundations, and by the US National Science Foundation (grant nos. PHY-1707875, PHY-1806672 and PHY-1912465).

Author contributions

A.D., C.D. and D.F.J.K. conceived the project. All authors contributed to the development of the methodology. A.D., C.D., D.F.J.K. and I.A.S. wrote the original draft of the paper. All authors reviewed and edited the manuscript.

Competing interests

The authors declare no competing interests.

Additional information

Supplementary information is available for this paper at https://doi.org/10.1038/s41550-020-01242-7.

Correspondence and requests for materials should be addressed to A.D.

Peer review information *Nature Astronomy* thanks Guglielmo Tino and the other, anonymous, reviewer(s) for their contribution to the peer review of this work.

Reprints and permissions information is available at www.nature.com/reprints.

Publisher's note Springer Nature remains neutral with regard to jurisdictional claims in published maps and institutional affiliations.

© The Author(s), under exclusive licence to Springer Nature Limited 2020